ISSN (Print) 1226-1750
ISSN (Online) 2233-6656
Journal of Magnetics 23(1), 27-34 (2018) https://doi.org/10.4283/JMAG.2018.23.1.027

An Improved Conformal Mapping Method for Static Angular Eccentricity Analysis of Axial Flux Permanent Magnet Machines

Baocheng Guo*, Yunkai Huang*, and Fei Peng

School of Electrical Engineering, Southeast University, Nanjing 210096, China

(Received 9 July 2017, Received in final form 7 November 2017, Accepted 30 January 2018)

This paper presents an improved and simple analytical model to study the static angular eccentricity of single stator single rotor axial-flux permanent-magnet (AFPM) machine. The magnetic flux densities in the air gap under normal and static angular eccentricity are calculated by using a combination of Maxwell's equations and Schwarz-Christoffel (SC) transformation. The original contribution of the model is that angular eccentricity is obtained without extra transformations. Thus the proposed approach is simpler than existing methods. The calculated back electromotive forces (EMFs) and cogging torque by the proposed method are compared with those obtained from the finite element (FE) model, the results show acceptable accuracy of the proposed method. In this way, the effectiveness of the proposed method is verified.

Keywords : improved analytical model, axial flux PM machines, cogging torque, static declined eccentricity

1. Introduction

Axial-flux permanent-magnet machines (AFPMMs) have been widely used in flywheel energy storage systems (FESSs) [1] because of high power density and momentum. They are also considered as a good candidate for electric vehicles (EV.) and hybrid electric vehicles (HEVs) [2] due to their compact mechanical structure. However, AFPMMs suffer from eccentricities occur in the manufacturing and assembling progress, because of the high axial force and the relative small contact area between the rotor and the shaft, especially for the single rotor single stator AFPM machines. Eccentricity causes an unbalanced magnetic force [4] and the mechanical vibration [4] during operation, which results in bearing faults, shaft deformation or even leads to scratch between the rotor and the stator.

Several methods are proposed in literatures to study the AFPMMs with eccentricities. Finite element (FE) or semi-FE models can precisely calculate the characteristics of eccentricities [5]. However, since the non-uniform airgap length is along with the radial direction, eccentricity condition of AFPMMs requires 3D FE model. Therefore, the FE models are very time-consuming.

Alternatively, analytical models (AMs) are time saving and are accurate enough. Therefore, AMs can be regarded as good choices for eccentricity investigation.

The AMs which consider the tangential component of air gap flux density can be classified into two general groups. The first group is subdomain approach, the main idea of this method is to solve the governing equations with the boundary conditions between each region. However, it is difficult to solve the eccentric boundary conditions of AFPMMs under Cartesian coordinates. The other group is conformal mapping (CM) method. The CM method obtains complex permeance function by transforming the slotless domain to the slot domain. It should be noted that the original CM model developed by Zarko [6] only considers one slot region and thus neglects the interaction between neighbor slots. The Schwarz-Christoffel (SC) method is developed based on the CM method and operated via Matlab toolbox [7].

With regards to the eccentricity research on AFPMMs, Mark Thiele study the cogging torque via FE approach [5], while Antonino investigated manufacturing dissymmetry effects based on field functions in order to reduce computational time [8]. Nevertheless, these models are still based on the FE method and time consuming. In [9], the author adopted the lateral force approach to study the static angular eccentricity considering slot effect. This

*Co-Corresponding author: Tel: +86-2583794169-807
Fax: +86-2583791696, e-mail: huangyk@seu.edu.cn
Tel: +8615005145661, Fax: +86-025-83794169-807
e-mail: guobaocheng1986@gmail.com

technique is convenient and simple. However, it neglects the tangential components of the air gap flux density. As previous study [10], and [11] deal with several types of eccentricities. However, the magnetic flux densities of the static declined eccentricity in [10] do not match very well with the FE results. The analytical model of static and dynamic axis eccentricity was presented in [11].

In this paper, an improved and simple analytical model to study the static angular eccentricity of single stator single rotor axial-flux permanent-magnet (AFPM) machine is proposed, and it is more improved than [10] for exactly modeling and calculating the flux densities in the air-gap. The magnetic flux densities in the air gap under normal and static angular eccentricity are calculated by using a combination of Maxwell's equations and Schwarz-Christoffel (SC) transformation. In this method, the angular eccentricity is obtained without extra transformation. Thus the proposed approach is simpler than existing methods.

This paper is organized as follows. Section 2 presents the AFPM machine investigated in this paper. In Section 3, the modeling process of magnetic distribution is introduced. The new technique considering static declined eccentricity is presented in Section 4. Section 5 discusses normal and eccentric results calculated by the proposed method as well as by the 3D FE model, which verify the accuracy of the proposed method. Lastly, conclusions are drawn.

2. The Investigated AFPMM Prototype

Figure 1 shows the construction of the investigated AFPMM.

This machine is a 5 phase, 2 pole pairs, 10-slot AFPMM, basic dimensions of this AFPMM are shown in Table 1. The quasi 2D approach in [11] is used to simplify the model. The average radius of the *i*-th layer is given by:

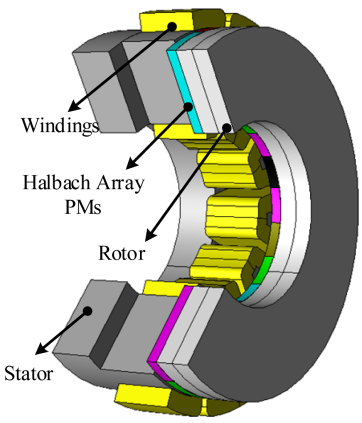

Fig. 1. (Color online) Construction of AFPM machine.

Table 1. Parameters of the 4-pole, 10-slot AFPMM.

Parameter	Symbol	Value	Unit
Rated power	P	20	kW
DC bus voltage	U	200	V
Rated speed	n_p	15,000	r/min
Number of poles / slots	p/Q_s	4/10	-
Stator outer radius	R_o	100	mm
Stator inner radius	R_i	50	mm
Air gap length	g_0	3	mm
Remnant flux density of PM	B_r	1.21	T
Permanent magnet	-	NdFeB	-

$$R_{ave}^{j} = R_i + \frac{R_o - R_i}{2n_s}(2j-1), \quad j = 1, 2, ..., n \tag{1}$$

$$t_{cp} = \frac{R_o - R_i}{n_s} \tag{2}$$

where n_s is the number of the slices, and t_{cp} is the width of the slices, R_i is the stator inner radius and R_o is the stator outer radius.

Six slices are selected to calculate the normal and defect conditions for acceptable accuracy.

3. Calculation of the Magnetic Field

A previous approach [12] is used to calculate the magnetic induction in the air gap caused by the magnets. The following assumptions are made to reduce the complexity of the calculation:

1) The magnetic material has uniform magnetization. The relative recoil permeability μ_r is constant with a value of unity in the air gap, as well as in the NdFeB materials.

2) Magnetic saturation is absent, and the rotor iron cores have infinite magnetic permeability.

3) Eddy current effects are neglected, which avoids the need for a complex eddy current field formulation.

3.1. Flux Density Calculation without slot

Based on [12], the magnetization vectors could be obtained using Fourier series method, the axial (M_z) and circumferential (M_θ) magnet magnetizations are shown in Fig. 2.

To solve the magnetic fields shown in Fig. 3, the magnetic vector potential A is used. In region I and II, take the slice of mean radius R_m as example, the Laplace equation (no source term) have to be solved using Cartesian coordinates:

$$\frac{1}{R_m}\frac{\partial^2 A}{\partial \theta^2} + \frac{\partial^2 A}{\partial z^2} = 0 \tag{3}$$

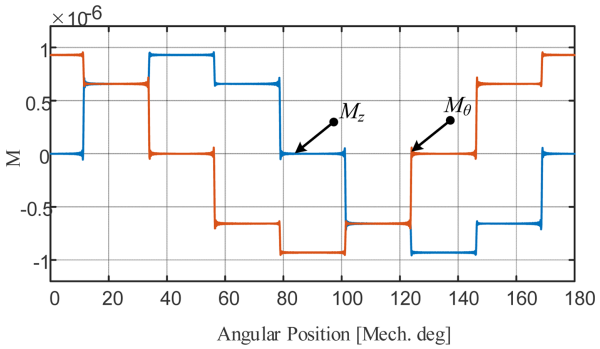

Fig. 2. (Color online) Axial and circumferential magnetization vectors.

Fig. 3. Model of slotless air gap flux.

Based on the separating variable method, the general magnetic vector potential solution for region I and II can be written as:

$$A_I = \sum_{n=1}^{\infty}\left(a_n^I \frac{\cosh(nz/R_m)}{\cosh(nz_1/R_m)} + M_n\cos(n\delta)\right)\cos(n\theta) + \sum_{n=1}^{\infty}\left(c_n^I \frac{\cosh(nz/R_m)}{\cosh(nz_1/R_m)} + M_n\sin(n\delta)\right)\sin(n\theta) \tag{4}$$

$$A_{II} = \sum_{n=1}^{\infty}\left(a_n^{II}\frac{R_m}{n}\frac{\cosh(n(z-z_2)/R_m)}{\sinh(n(z_1-z_2)/R_m)}\right)\cos(n\theta) + \left(c_n^{II}\frac{R_m}{n}\frac{\cosh(n(z-z_2)/R_m)}{\sinh(n(z_1-z_2)/R_m)}\right)\sin(n\theta) \tag{5}$$

where n is the harmonic order, M_n is a combined magnet magnetization consists M_z and M_θ, δ is the initial phase angle between the rotor and the stator.

The coefficients (a^I_n, c^I_n, a^{II}_n, c^{II}_n) in these regions can be determined using the following boundary conditions:

$$\begin{cases} H_{\theta I}(\theta, z)\big|_{z=z_0} = 0 \\ H_{\theta II}(\theta, z)\big|_{z=z_2} = 0 \\ H_{\theta I}(\theta, z)\big|_{z=z_1} = H_{\theta II}(\theta, z)\big|_{z=z_1} \\ A_{\theta I}(\theta, z)\big|_{z=z_1} = A_{\theta II}(\theta, z)\big|_{z=z_1} \end{cases} \tag{6}$$

By solving Eq. (6) numerically, the magnetic fields can be deduced:

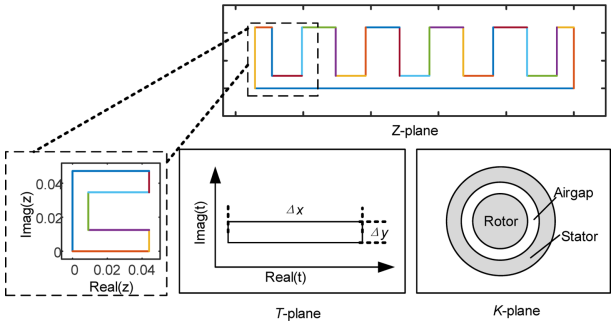

Fig. 4. (Color online) SC mapping on different planes.

$$B_z = \frac{1}{R_m}\frac{\partial A}{\partial \theta} \qquad B_\theta = \frac{\partial A}{\partial z} \tag{7}$$

3.2. Flux Density Calculation with slot

The effect of stator slotting is considered using numerical SC mapping technique [13]. For AFPMMs, the complex relative air gap permeance (λ^*) is calculated as:

$$\lambda^* = \frac{\partial K}{\partial T}\cdot\frac{\partial T}{\partial Z}\cdot\frac{1}{\lambda_0} = \lambda_Z + j\cdot\lambda_\theta \tag{8}$$

where λ_0 is the complex permeance in the slotless air gap T-plane, while λ_z and λ_θ are the axial and circumferential components of the relative air gap permeance in the original Z-plane. K, T, and Z represent the K-plane, T-plane, and Z-plane, respectively, as shown in Fig. 4. Notice that it is necessary to introduce the K-plane in order to calculate the Hague's solution.

The SC mapping is used firstly to convert the polygon in Z-plane to the canonical rectangle in T-plane. After reaching annular domain (K-plane), Hague's solution is then used to calculated the field in K-plane. Afterwards, the final permeance function is calculated by Eq. (8) and the flux density in the slot region is:

$$B_z = B_t\cdot\lambda^* = (B_z + j\cdot B_\theta)\cdot(\lambda_z + j\cdot\lambda_\theta) \tag{9}$$

4. Proposed Model of Eccentricity

The description of static angular eccentricity is shown in Fig. 5. r is the maximum distance that the points at the mean radius R_m is biased from the normal air gap length g_0. The permanent magnet height is h_m. The eccentricity can be described by static eccentricity factor (SEF) which shows the eccentricity level as r/g_0.

The influence of eccentricity is that it changes the airgap length at different radius. Thus, the flux distribution varies accordingly. The airgap length at any radius R can be obtained by the following formula:

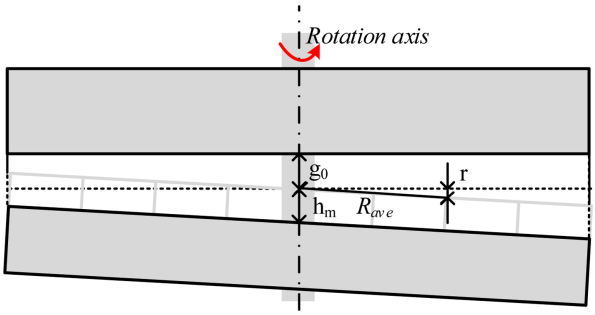

Fig. 5. (Color online) Configuration of static declined eccentricity.

$$g(R,\ \varphi) = g_0\left(1 - \frac{R}{R_m}\frac{r}{g_0}\cos(\varphi - \gamma_0)\right) \tag{10}$$

where φ is the angle from the reference point (γ_0) with the minimal air gap.

In this paper, to improve the accuracy of the magnet flux calculation, the structure of static angular eccentricity is directly draw by the SC Matlab toolbox as shown in Fig. 6. In order to reduce the computational time, the flux densities within only half period is calculated.

Afterwards, the permeance function could be calculated according to Eq. (8). It is necessary to mention that the λ_0 is the value obtained from normal condition, the complete permeance function of whole slots is subsequently calculated based on the symmetric boundary condition.

The λ_z and λ_θ are shown in Fig. 7.

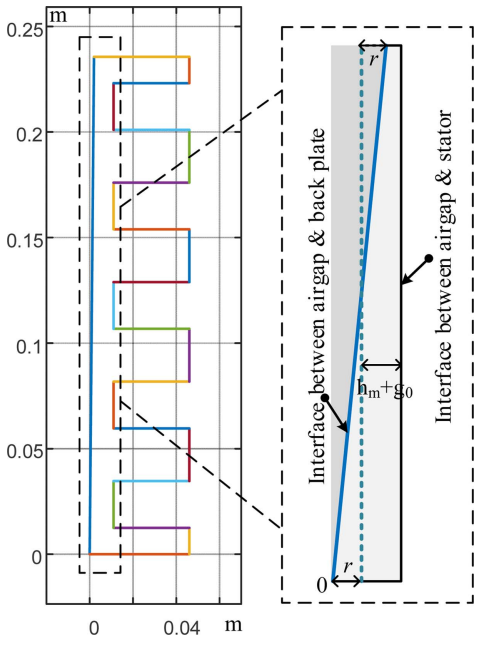

Fig. 6. (Color online) Configuration of static declined eccentricity.

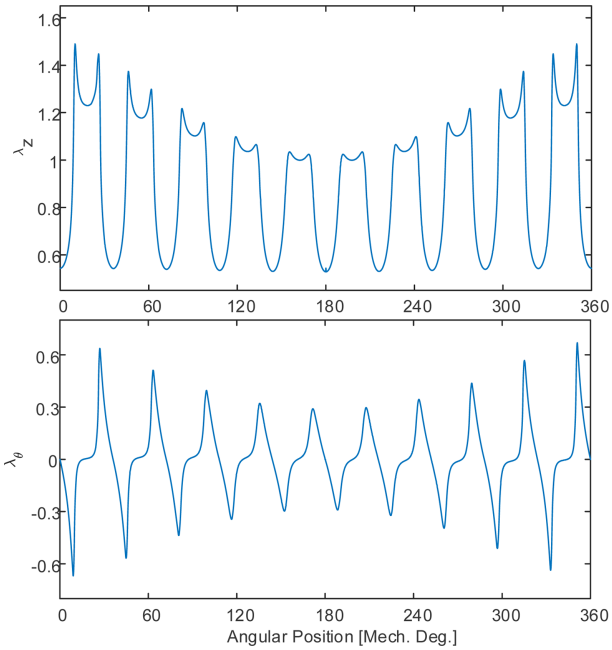

Fig. 7. (Color online) Permeance function. (a) Real part λ_z and (b) imaginary part λ_θ.

5. Results and Discussion

An FE model of the investigated AFPMM is built to validate the proposed method. Since the described defect is asymmetric, the FE model includes the complete geometry.

Since the stator of this machine is open slot, it is necessary to introduce the winding function theory to calculate the flux linkage, as:

$$\psi_{c,i} = \frac{R_{ave,i}(R_o - R_i)}{n_s}\int_0^{2\pi} F_{Dc}B_{z,i}d\theta \tag{11}$$

where $B_{z,j}$ is the axial component of the flux density in the j_{th} layer, F_{Dc} is the distribution function of coil, if the θ_b and θ_{so} represent the coil opening and slot opening. The coil distribution function could be found in [14] and its expression is given by:

$$F_{Dc}(\theta) = \begin{cases} 0 & \text{for: } \theta \in [-\pi;\ -(\theta_b + \theta_{so})/2] \\ (N_c/\theta_{so})\,(\theta_b + (\theta_b + \theta_{so})/2) & \\ & \text{for: } \theta \in [-(\theta_b + \theta_{so})/2;\ -(\theta_b - \theta_{so})/2] \\ N_c & \text{for: } \theta \in [-(\theta_b + \theta_{so})/2;\ (\theta_b + \theta_{so})/2] \end{cases} \tag{12}$$

Afterwards, the total flux linkage of one phase is obtained by adding the fluxes of all coils belonging to this phase. The coil configuration should be taken account in

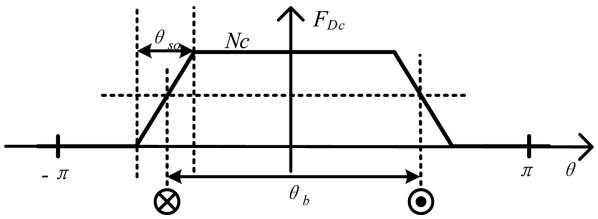

Fig. 8. Distribution function of coil.

this stage. The back EMF in the i_{th} layer $E_{A,j}$ for phase A, is obtained as

$$E_{A,i} = -\frac{d\psi_k}{dt} \tag{13}$$

The cogging torque is calculated by using Maxwell stress tensor method. This method is applied at the center of the air gap and can be expressed as

$$T_{cog} = \frac{R_o^3 - R_i^3}{3\mu_0} \int_0^{2\pi} B_z B_\theta d\theta \tag{14}$$

The axial force can be expressed as:

$$F_a = \frac{R_o^2 - R_i^2}{4\mu_0} \int_0^{2\pi} (B_z^2 - B_\theta^2)\, d\theta \tag{15}$$

5.1. Normal Conditions

The calculated air gap flux densities at no-load of the healthy machine by the proposed method and FE method are shown in Fig. 9. It is shown that the axial component (B_z) of flux density field matches well. There is little RMS error between the circumferential component (B_θ) and FE model. The maximum error is 17.9 % for circumferential component, which is acceptable.

In Fig. 10, the calculated flux linkage and the back EMFs of coil A by the proposed method and FE method are compared. They also matched very well.

By neglecting the saturation, the cogging torque can be calculated from no-load magnetic field. The axial force and the cogging torque have same period and can be expressed as *Cogging torque period* = $2\pi/LCM$ (Q_s, $2p$). Figure 11 shows the cogging torque and axial force in one period. It shows a good correspondence between FEM and analytical model for cogging torque, but the error of axial force is large.

Table 2. Comparison of the flux density (RMS value) of normal condition.

	B_z	B_θ	Unit
FE model	0.5287	0.1589	T
Analytical model	0.5532	0.1303	T
Error	4.6	17.9	%

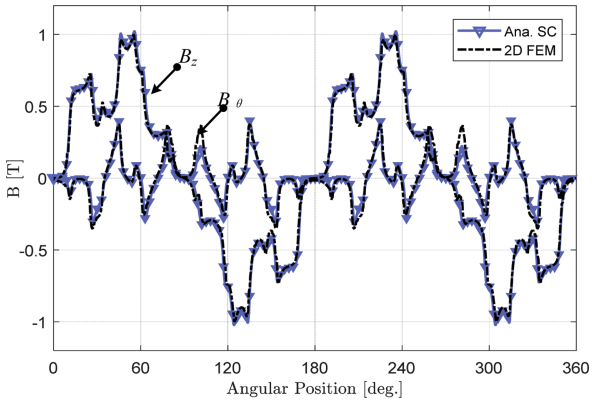

Fig. 9. (Color online) Analytical and FEM flux density field for healthy condition.

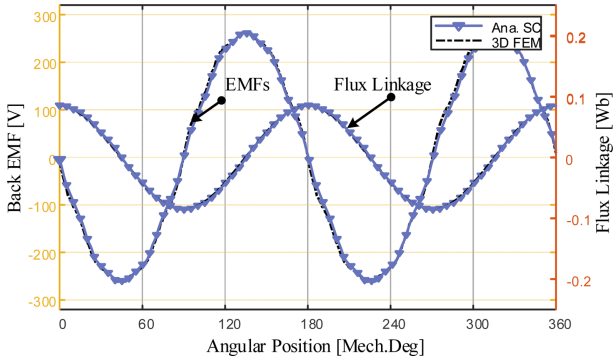

Fig. 10. (Color online) Back EMF of phase A and flux linkage of coil A (A1 and A2) for healthy condition.

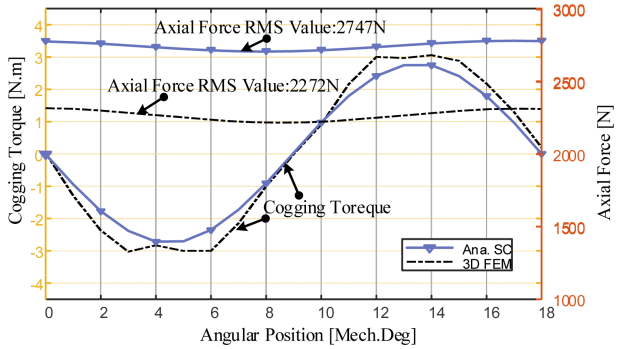

Fig. 11. (Color online) Cogging torque and axial force for normal condition.

5.2. Static Defect Calculation

Figure 12 presents the flux densities under static defect condition. r is set as 1mm, the flux densities at the mean radius are calculated by both the proposed method and FE method. Good agreement of both B_z and B_θ are shown in

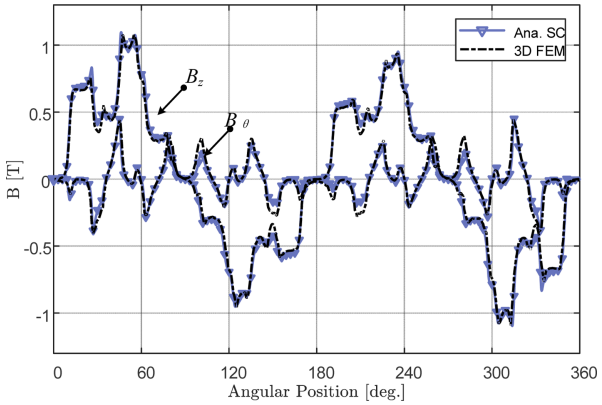

Fig. 12. (Color online) Analytical and FEM flux density field for eccentricity condition.

Table 3. Comparison of the flux density (RMS value) of defect condition.

	B_z	B_θ	Unit
FE model	0.5331	0.1531	T
Proposed AM	0.5504	0.1220	T
Error	3.2	20.3	%

Fig. 12, the RMS errors are shown in Table 3, which maintain the same level as the normal condition and thus the results are acceptable. It should be noted that the declined position does not vary with rotation, which means that the permeance function obtained in section 4 does not change when studying the dynamic case.

The results of back EMF and flux linkage of the eccentricity model are almost the same compared to those of the normal condition model as shown in Fig. 13. Notice that the investigated machine in this paper has two pole-pairs, the two coil in one phase are connected in parallel. Therefore, the variable air gap length results in increase of flux linkage in one winding (A1), while decrease in another (A2). Thus, the same final flux

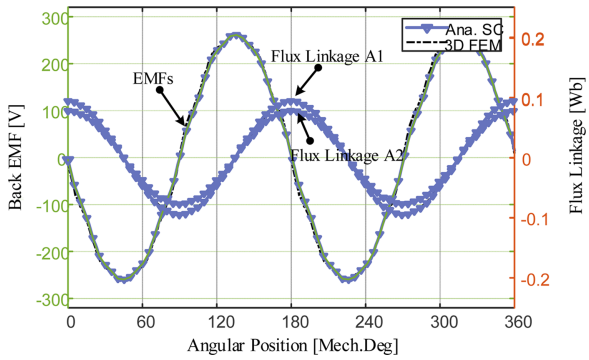

Fig. 13. (Color online) Back EMF of phase A and flux linkage of coil A1 and A2 for eccentricity condition.

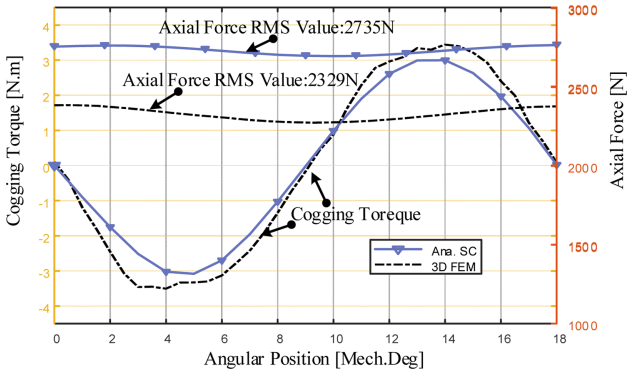

Fig. 14. (Color online) Cogging torque and axial force for eccentricity condition.

linkage value as normal condition as the normal condition is obtained in the end.

Figure 14 shows the cogging torque and axial force for eccentricity condition. It is shown that the eccentricity has little influence on the axial force, however, the cogging torque is slightly increased.

Compared with the FE method, cogging torque calculated by the proposed method has lower peak value. The cogging torque calculation has a strong interaction with circumferential component, although the method proposed in this paper has improved the accuracy of axial component, it still difficult to predict circumferential component at satisfactory accuracy. Nevertheless, it has been shown that this analytical method is able to predict the trend for static declined condition.

5.3. Comparison

Table 4 shows the second norm of the error between the axial and circumferential flux densities under defect condition of the proposed model and previous model. It is obvious that the proposed model in this paper has improved the accuracy.

Another important issue should be considered is the calculation time. All the computations were done on a PC with Intel core i7 processor and 32Gb of memory.

As for the AM model, the transformation of a polygon in the Z plane (24 points) to the canonical rectangle plane takes most of the computation time, almost 3 seconds. The global quantities such as EMFs and cogging torque, can be calculated in a very little time. The proposed

Table 4. Comparison of the flux density between proposed model and previous model.

	$\|(B_{z,AM}-B_{z,FEM})\|_2$	$\|(B_{\theta,AM}-B_{\theta,FEM})\|_2$
Proposed model	1.24	0.95
Model in [9]	2.13	1.03

analytical model in this paper use 200th harmonic orders for the calculation of the PM and air gap region, it requires 5.02 seconds to obtain the global quantities within one mechanical cycle. The computation time of defect condition takes almost the same time as that of the normal condition.

The FEM was created by commercial software JMAG, the 3D FE model consists 104,897 triangular elements. The solution type is transient with 361 steps for one mechanical period. The 3D FE model requires almost 5 hours to obtain the results for one electrical period.

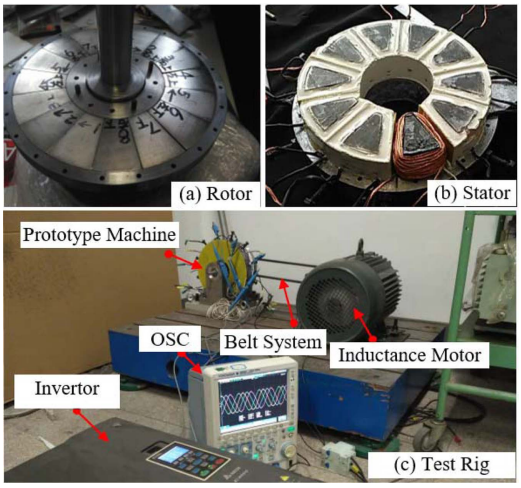

Fig. 15. (Color online) The prototype machine and the test rig.

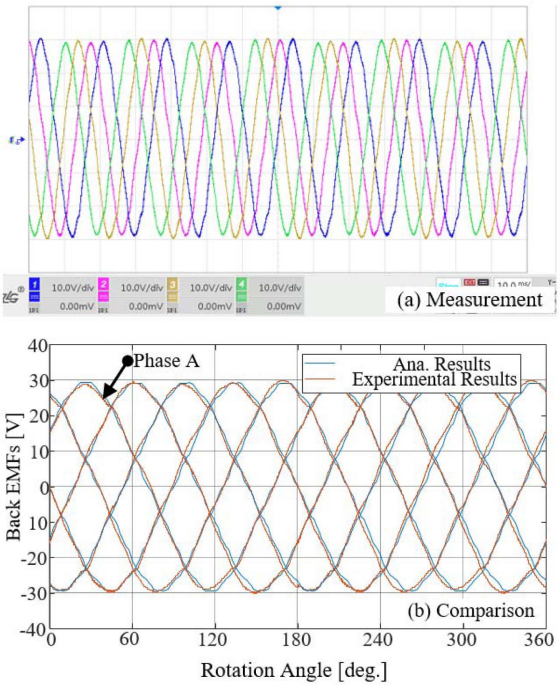

Fig. 16. (Color online) Back EMFs measurement and comparison.

6. Experimental Results

The rotor disk and the stator of the AFPM prototype are shown in Figs. 15(a) and (b), respectively. The experimental setup and devices are shown in Fig. 15(c). In the test bench, the prototype is coupled with an inductance motor via belt system. The inductance motor is driven by an invertor.

With regards to the experiment, a no-load test was done at 1500 rpm. The back EMFs under normal condition were recorded, as shown in Fig. 16(a). The comparsion between analytical results and measurement is shown in Fig. 16(b), and it can be seen that the results match well.

7. Conclusion

This paper has presented an improved approach for modeling AFPMMs with stator declined eccentricity. The back EMFs, cogging torque, axial force have been compared with the results of the 3D FE model. It is shown that the computation time is reduced remarkably while maintaining high accuracy at the same level as the FE model.

The contributions of this paper include modeling static declined eccentricity using SC Matlab toolbox directly and the permeance function of defect condition could be used to calculate the flux densities, therefore the method can also be used to calculated the dynamic eccentricity. Moreover, the single rotor single stator AFPM machine has been investigated in this paper, the defect condition mentioned in this paper has little influence on back EMFs because of compensation of flux linkages.

Acknowledgment

This work is supported in part by the National Nature Science Foundation of China (Project Number 51777034).

References

[1] T. D. Nguyen, K.-J. Tseng, S. Zhang, and T. D. Nguyen, IEEE Trans. Ind. Electron. **58**, 3784 (2011).
[2] Polikarpova, M., P. Ponomarev, P. Lindh, I. Petrov, W. Jara, V. Naumanen, J. A. Tapia, and J. Pyrhonen, IEEE Trans. Ind. Electron. **62**, 12 (2015): 7382-90. https://doi.org/10.1109/TIE.2015.2465354.
[3] S. M. Mirimani, A. Vahedi, and F. Marignetti, IEEE Trans. Magn. **48**, 143 (2012).
[4] J. Li, R. Qu, and Y.-H. Cho, in 2014 International Conference on Electrical Machines (ICEM), (2014) pp 502-

508.
[5] T. Mark, doctoral, Charles Darwin University (2013).
[6] D. Zarko, D. Ban, and T. A. Lipo, IEEE Trans. Magn. **45**, 2943 (2009).
[7] E. Ilhan, E. T. Motoasca, J. J. Paulides, and E. A. Lomonova, Math. Sci. **6**, 1 (2012).
[8] A. Di Gerlando, G. M. Foglia, M. F. Iacchetti, and R. Perini, IEEE Trans. Magn. **48**, 1995 (2012).
[9] K. Abbaszadeh and A. Rahimi, Sci. Iran. Trans. Comput. Sci. Eng. Electr. **22**, 2482 (2015).
[10] B. Guo, Y. Huang, F. Peng, Y. Guo, and J. Zhu, IEEE Trans. Magn. **53**, 1 (2017).
[11] G. Baocheng and H. Yunkai, J. Magn. **21**, 554 (2016).
[12] P. Jin, Y. Yuan, H. Lin, S. Fang, and S. L. Ho, J. Magn. **18**, 95 (2013).
[13] D. Zarko, D. Ban, and T. A. Lipo, IEEE Trans. Magn. **42**, 1828 (2006).
[14] H. Tiegna, A. Bellara, Y. Amara, and G. Barakat, IEEE Trans. Magn. **48**, 1212 (2012).